Evaluating P-Band TomoSAR for Biomass Retrieval in Boreal Forest

Evaluating P-Band TomoSAR for Biomass Retrieval in Boreal Forest

Erik Blomberg, Lars M. H. Ulander, *Fellow, IEEE*, Stefano Tebaldini, *Senior Member, IEEE*, and Laurent Ferro-Famil, *Member, IEEE*

***Abstract*— P-band synthetic aperture radar (SAR) is sensitive to above-ground biomass (AGB) but retrieval accuracy has been shown to deteriorate in topographic areas. In boreal forest, the signal penetrates through the canopy to interact with the ground producing variations in backscatter depending on ground topography, forest structure, and soil moisture. Tomographic processing of multiple SAR images Tomographic SAR (TomoSAR) provides information about the vertical backscatter distribution. This article evaluates the use of P-band TomoSAR data to improve AGB retrievals from backscattered intensity by suppressing the backscattered signal from the ground. This approach can be used even when the tomographic resolution is insufficient to resolve the vertical backscatter profile. The analysis is based on P-band data from two campaigns: BioSAR-1 (2007) in Remingstorp, southern Sweden, and BioSAR-2 (2008) in Krycklan (KR), northern Sweden. BioSAR airborne data were also processed to correspond as closely as possible to future BIOMASS TomoSAR acquisitions, with BioSAR-2-based results shown. A power law AGB model using volumetric HV polarized backscatter performs best in KR, with training residual root mean-squared error (RMSE) of 30%–36% (27–33 t/ha) for airborne data and 38%–39% for simulated BIOMASS data. Airborne TomoSAR data suggest that both vertical and horizontal tomographic resolution are of importance and that it is possible to greatly reduce AGB retrieval bias when compared with airborne P-band SAR backscatter intensity-based retrievals. A lack of significant ground slopes in Remningstorp reduces the benefit of using TomoSAR data which performs similar to retrievals based solely on P-band SAR backscatter intensity.**

***Index Terms*— Biomass, boreal forest, P-band, tomography.**

I. Introduction

THE forests of Earth cover 31% of the land surface [1] and play a crucial role in both local and global ecosystems, containing a majority of the biodiversity and providing an almost endless variation in biotopes. Reliable, accurate, and inexpensive monitoring of forest parameters is essential to provide input for forest managers, policy makers, and researchers. This can only be achieved on a large scale by spaceborne remote-sensing tools capable of global coverage. Of special interest is accurate global monitoring of above-ground biomass (AGB), the theoretical dry mass of all living plant matter above the ground surface. Changes in AGB are directly related to the health and productivity of the forest and its significant role in the global carbon cycle.

Optical data have formed the baseline by providing information of coverage and the multispectral response of the canopy which can be related to forest type, structure, and health through correlation with inventory data. Optical sensors are however dependent on solar illumination and severely impacted by cloud cover, limiting the spatial and temporal coverage. Optical wavelengths mostly interact with the top of the canopy and exhibit decreasing sensitivity to AGB with increasing forest density, saturating at 15–70 t/ha [2].

Radar operating in the microwave frequency atmospheric window is an active sensor and is mostly unaffected by weather, with the limiting factor often being data downlink and frequency allocations. High-resolution images provided by synthetic aperture radar (SAR) are increasingly being used for mapping forest and estimating AGB. Shorter wavelengths such as X-band interact mainly with the upper canopy while longer wavelengths are able the penetrate deeper into the forest volume and have higher sensitivity, at the cost of more complex scattering mechanisms [3], [4]. Different techniques can improve AGB retrievals by providing more information about the forest structure such as the distribution of branch size and orientation relative to the stems. Polarimetric SAR (PolSAR) measures the different polarimetric components of the backscattered signal while interferometric SAR (InSAR) and tomographic SAR (TomoSAR) generate interferometric height and tomographic profiles by processing SAR images from multiple sensors. For longer wavelengths such as L-band and P-band, the forest backscatter remains correlated over longer periods of time and it is possible to use repeat acquisitions [5]–[9].

P-band wavelengths are of special interest for spaceborne remote sensing of forest as they represent the lowest frequencies that are not severely affected by transmission through the atmosphere and ionosphere. There are currently no P-band SAR satellites but ESA's upcoming P-band BIOMASS mission specifically targets measurements of global forest

Manuscript received April 26, 2019; revised December 7, 2019 and April 6, 2020; accepted April 17, 2020. Date of publication September 22, 2020; date of current version April 22, 2021. This work was supported by the European Space Agency through BIOMASS L2 Implementation Study under Contract 4000119231. *(Corresponding author: Erik Blomberg.)*

Erik Blomberg and Lars M. H. Ulander are with the Department of Space, Earth and Environment, Chalmers University of Technology, 41296 Gothenburg, Sweden (e-mail: erik.blomberg@chalmers.se).

Stefano Tebaldini is with the Dipartimento di Elettronica, Informazione e Bioingegneria, Politecnico di Milano, 20133 Milano, Italy.

Laurent Ferro-Famil is with IETR Laboratory, UMR CNRS 6164, University of Rennes 1, 35042 Rennes, France.

Color versions of one or more of the figures in this article are available online at https://ieeexplore.ieee.org.

Digital Object Identifier 10.1109/TGRS.2020.3020775

TABLE I
SUMMARY OF STAND AND PLOT DATA FROM RE AND KR. PERCENTAGES ARE RELATIVE MEAN AGB

Site	N	Type	Main source of AGB data	Mean AGB [t/ha]	AGB range [t/ha]	Area [ha]	Error
RE	10	Square plots	Plot-level measurements	181	52-267	0.66-0.69	A few percent
	58	Stands	Stem volume map	121	9-211	0.50-9.4	25 t/ha
	148	Circular plots	NA	-	-	0.79	-
KR	26	Stands	Plot-level measurements	93	23-183	1.5-22	4-21 %
	517	Circular plots	AGB map	77	5-268	0.79	16 %

AGB and will have a repeat pass tomographic mode [10]. AGB retrieval using P-band SAR data have produced good results for boreal forest but retrieval accuracy deteriorates for topographic areas [7], [11]–[13]. Improving retrievals through either physics based or empirical modeling of topographic effects has proven challenging as the backscattered power is highly sensitive to relatively small-scale variations and even when high-resolution digital terrain model (DTM) data are available models struggle to productively incorporate more than a single ground slope parameter [14], [15].

P-band TomoSAR has been used to improve AGB retrieval in high AGB tropical forest. For example, analysis of P-band tomographic data from the TropiSAR campaign in Paracou, French Guiana, have demonstrated a significantly improved sensitivity between backscatter at the 30-m above ground level (AGL) level and biomass in tropical forest [16], [17]. This work evaluates how tomographic processing of P-band SAR data can be used to improve AGB retrievals from boreal forest and highlights the limitations set by the vertical resolution available. Following this introduction, Section II presents the two radar and forest parameter data sets used while Section III details the tomographic processing and retrieval methodology. Results are found in Section IV with Sections V and VI providing discussion and conclusions, respectively.

II. EXPERIMENTAL DATA

This analysis is based on the P-band SAR images acquired using DLRs airborne E-SAR system as part of the BioSAR-1 and BioSAR-2 campaigns. These were two of a set of campaigns designed to support future L- and P-band SAR satellite missions with regard to boreal forest measurements, with a focus on the successful selection of BIOMASS for ESAs seventh Earth Explorer mission. Both campaigns targeted well-characterized forestry test sites in Sweden and include radar data as well as extensive *in situ* measurements of forest parameters and high-resolution airborne lidar scans [18], [19].

The forest data used is summarized in Table I and represents a combination of all relevant data sets available to maximize the area covered. Some stands and plots have individual measurements and estimates of AGB, and are used for validation while other sets use AGB derived from a recalibrated stem volume map or a lidar-based AGB map. The accuracies of these are harder to quantify and they are therefore used for training, potentially giving slightly worse model fits but more reliable error estimates. Care has been taken that no data sets overlap spatially but the diverse methods used makes a rigorous error analysis difficult.

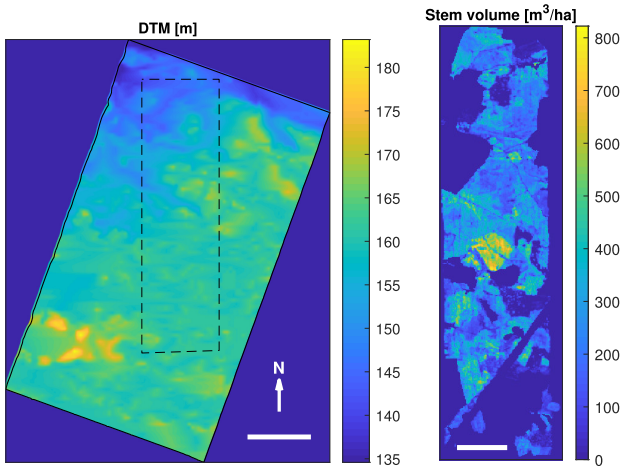

Fig. 1. RE (a) DTM and (b) stem volume map based on ALS data and *in situ* measurements. White scale bars represent 1 km and 500 m, respectively, and the black dashed outline shows the ALS coverage.

A. BioSAR-1, 2007

Remningstorp (RE) is a forestry test site located in the south of Sweden (Lat. 58° 28' N, Long. 13° 38' E) in relatively flat terrain as seen in Fig. 1(a). The hemiboreal forest represent a transition between the temperate to the boreal zones and consists mostly of well-managed stands of Norway spruce, *Picea abies*, Scots pine *Pinus sylvestris*, and some birch *Betula spp.* with smaller areas of other species. A number of stands and plots were visited throughout the BioSAR-1 campaign and *in situ* measurements were complemented by airborne lidar scanning (ALS) on April 24, 2007 covering a central strip of the area of interest running north to south.

Fully polarimetric P-band radar data were acquired on three separate occasions in 2007 to capture temporal variations: March 9, April 2, and May 2. The P-band baselines intended for tomographic processing were spread out evenly with three flight tracks on each date (with the addition of the master track being flown at the later dates as well). The end result is nine images covering the area marked by the black outline in Fig. 2, obtained in a left-looking geometry on a flight heading of 200° [18].

BioSAR-1 data includes AGB based on *in situ* measurements on individual trees for ten roughly square (80 m × 80 m) plots. These plots were used in [12] (denoted INS), together with 58 forest stands (denoted LID) for which AGB estimates were produced from the ALS-derived stem volume map shown

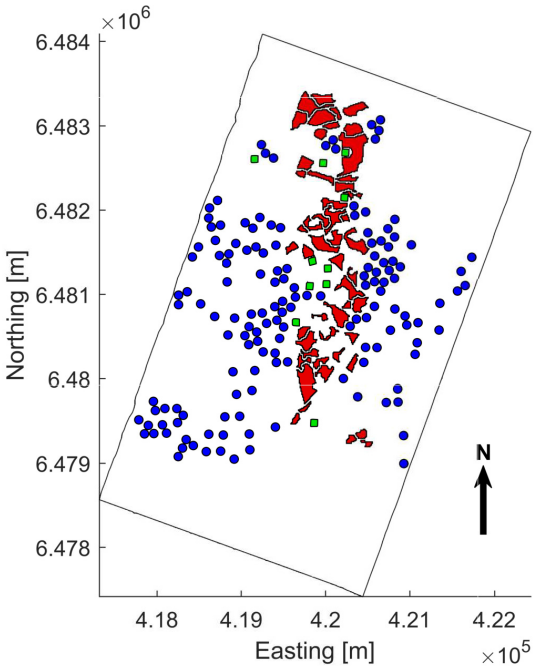

Fig. 2. Map of the P-band SAR data coverage in RE (black outline), with ten square plots for which AGB values are based on measurements of each tree (green) and 50 stands with AGB estimates based on ALS data and *in situ* measurements (red) [11]. The 148 circular plots (blue) are used to study the influence of ground slope.

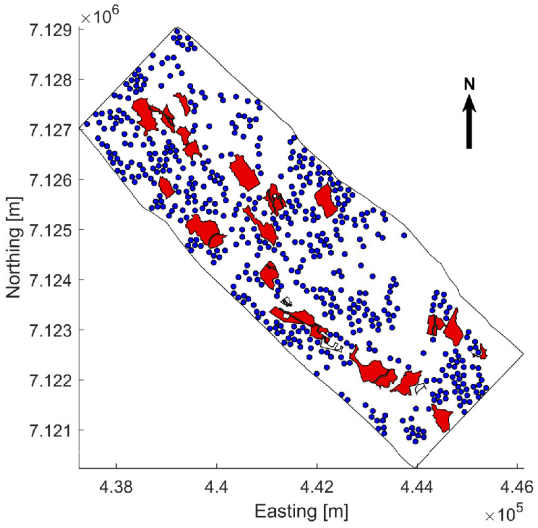

Fig. 3. Map of the P-band SAR data coverage in KR (black outline), with 26 *in situ* forest stands (red) and 517 circular plots (blue).

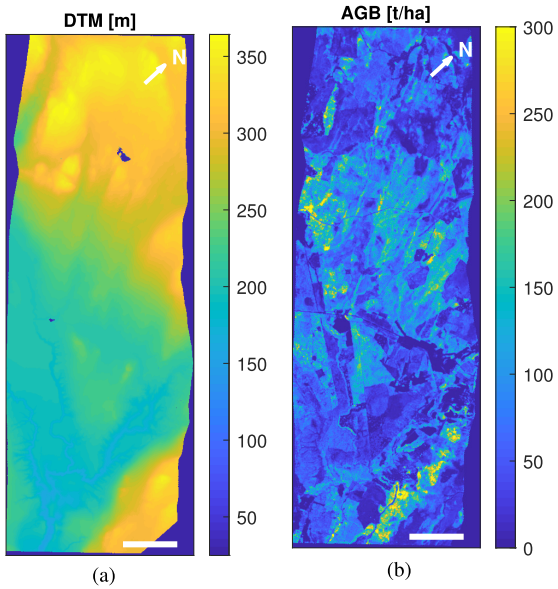

Fig. 4. KR (a) DTM and (b) AGB data based on ALS data and *in situ* measurements. White scale bars represent 1 km.

in Fig. 1(b) and field measurements [11]. All 10 square plots and 50 of the forest stands, shown in Fig. 2 in green and red, respectively, are used for this analysis. Eight of the original forest stands were excluded due to overlap with the square plots.

An extra set of 148 circular 50-m radius plots, shown in blue in Fig. 2, were generated using the procedure introduced in [11] for KR: plots are randomly placed within homogeneous forest stands while maximizing the number of plots, minimizing topographical variation within each plot and maintaining a minimum 10-m separation between plots. These circular plots provide an expanded set of backscatter values for investigating the effects of ground slope. Both the topographic variation and ground slopes were calculated from the DTM in Fig. 1(a). Table I includes a summary of the plots and stands in RE.

B. BioSAR-2, 2008

The 2008 BioSAR-2 campaign targeted the KR forestry research site, located in the north of Sweden (Lat. 64° 14' N, Long. 19° 50' E). KR has a pronounced topography and is covered by boreal forest (mostly Norway spruce, *Picea abies*, and Scots pine *Pinus sylvestris*) of varying density. During BioSAR-2 a set of 31 forest stands were selected and stand estimates of forest AGB values were calculated from *in situ* measurements of tree diameter at breast height, tree height, age, and species. The data were collected from a regular grid of 10-m radius circular plots with about ten plots per stand, enabling a statistical estimate of the error in the resulting stand biomass values [19], [20]. About 26 of these stands provide stand-level AGB within the coverage of the radar images and are shown in red in Fig. 3. These are a subset of the 29 stands denoted INS in [12], with three stands excluded due to not being fully covered by the TomoSAR data set.

High-resolution helicopter-based lidar data were obtained in parallel with the ground campaign resulting in a 0.5 m × 0.5 m resolution DTM and digital surface/canopy model (DSM/DCM). Fig. 4(a) shows the DTM for the area of interest while Fig. 4(b) shows a biomass map, generated from the DCM using the *in situ* plot measurements complemented by a further 110 plots [12], [19]. The 517 plots marked blue in Fig. 3 are the same 50-m radius circular plots used in [21] and were obtained using to the methodology described in [11]. This approach of randomly selecting nonoverlapping plots within forest stand boundaries was also used to select the 97 plots denoted LID in [12] although the set used here was

TABLE II
SUMMARY OF TOMOSAR PARAMETERS [18], [19]

	BioSAR 1	BioSAR 2
Number of headings	1	2
Flight tracks per heading	9	6
Baseline spacing	10 m	8 m
Baseline orientation	Horizontal	Horizontal
Average flight altitude (AGL)	3888 m	3891 m
Incidence angle θ	25° - 53°	24° - 53°
Vertical resolution δ_z	10 m - 52 m	21 m - 104 m

generated separately. AGB values used for model training are obtained by averaging biomass map values within each plot.

BioSAR 2 radar images were acquired using the E-SAR system, with the P-band data used here coming from a single flight on the 14th of October. The flight followed a race track path, imaging a 3 km $\times$ 10 km scene in a left looking geometry while displacing each subsequent pass horizontally. The result was two sets of six fully polarimetric images, with the first comprised of north-east looking images from a flight heading of 134° and the second looking south-west from a flight heading of 314° [12], [19]. These data sets are in this article denoted NE and SW, respectively.

III. METHODOLOGY

A. Tomographic Processing

Tomography is the extension of the 1-D SAR aperture into a 2-D aperture, thereby providing information about the illuminated scene resolved in all three spatial dimensions. Implementing TomoSAR is challenging due to practical considerations with the design and operation of SAR systems. As they generally only capture data along one flight line simultaneously, the resulting 2-D apertures are as a rule sparse in the extra dimension, limiting vertical resolution and introducing ambiguities [5].

This is compensated for by the limited vertical extent of relevant scenes for airborne TomoSAR. Multiple flight lines are captured at multiple time points (repeat passes for satellites) leading to decorrelation between subsequent images and the requirement that the variability of the backscatter phase from the imaged volume is limited to fractions of a wavelength. Tomographic inversion is however often possible as long as the acquisitions show good pairwise correlation [22].

In the case of BioSAR-1 and BioSAR-2, the airborne acquisitions were planned with consideration to the evaluation of future tomographic modes for BIOMASS. As can be seen from Table II, the two campaigns involve very similar geometries with BioSAR-2 using a shorter baseline spacing to increase the separation of ambiguities and expand the vertical extent of the resolved volume due to the larger differences in ground height at the site. In combination with the lower number of baselines, this limits the vertical resolution δ_z which therefore is not as good as for BioSAR-1, as seen in Table II. The large span in δ_z is due to the airborne geometry and corresponding variation in incidence angle and will be less pronounced for a spaceborne SAR. However, the reduced range resolution due to the low bandwidth of BIOMASS (6 MHz) will set a lower bound for δ_z to 20 m, corresponding to a maximum useful baseline of roughly 4600 m [17].

If the airborne acquisitions have a significantly better vertical resolution it is possible to reprocess the resulting tomograms to have a resolution cell size and orientation corresponding to the BIOMASS geometry and performance. This method can however not change the incidence angle dependence of the original airborne tomographic intensity. An example of simulated BIOMASS tomograms based on TropiSAR data is found in [17]. For the BioSAR data sets, the vertical resolution is not sufficient to fully emulate the spaceborne geometries except for the near range region of the BioSAR 1 scene. The simulated BIOMASS TomoSAR data sets have the correct bandwidth (through filtering in the frequency domain) but exhibit a larger range of incidence angles and vertical resolution. The best approximation of BIOMASS is found at near range.

The tomographic processing starts with complex images that have been phase calibrated and coregistered in the same slant range geometry. These can then directly form pairwise interferograms from which the vertical tomographic intensity profiles are generated using a Fourier beamformer. The resulting tomograms are then transformed from slant range geometry to ground range and then geocoded.

B. SAR and TomoSAR Observables

A common normalization for P-band SAR backscatter is $\gamma^0 = \sigma^0/\cos(\theta_i)$, where σ^0 is the surface area normalized backscatter coefficient and θ_i the local incidence angle. The intent is to compensate for the incidence angle-dependent backscatter from a forest canopy layer on sloping ground [23], [24]. All SAR data used in this article are γ^0 values derived from the original calibrated SAR image intensities together with incidence and ground slope angles computed from the corresponding geometries and DTMs.

TomoSAR generates a vertical backscatter intensity profile $I(z)$ for each horizontal pixel, where z in this case is normalized to height above ground. Any number of parameters with potential for AGB correlation could be obtained from such a profile if the forest volume is well resolved. However, this is not the case in neither RE nor KR where the forest height is generally less than the vertical resolution.

The improvement in AGB retrievals seen in [21] using L-band tomographic data came from suppressing the backscatter originating at ground level by integrating the vertical intensity profile above a $z = 10$ m threshold. This approach is here repeated at P-band with the volumetric tomographic backscatter intensity $I_{\text{vol}} = (1/40\ \text{m}) \int_{z=10\,\text{m}}^{z=30\,\text{m}} I(z)dz$. I_{tot} and I_{ground} are included for comparison, representing the total integrated tomographic backscatter (limited by the $z = -10$ m to $z = 30$ m extent of the processed data) and the ground level tomographic backscatter ($z = -10$ m to $z = 10$ m). Normalizing the integral by the total vertical extent produces the corresponding average of the tomographic profile with values generally close to the SAR image intensity while the shared normalization results in I_{tot} being the sum of I_{vol} and I_{ground}.

This is the same threshold used at L-band in [21] and was found to work well for this data set as well, with thresholds of roughly $z = 7.5$ m to $z = 15$ m showing decreasing volumetric intensity values with higher threshold but little variation in AGB dependence. It is worth noting that suppression of the ground backscatter is incomplete as the 10-m height cut-off is only half the best case resolution.

C. AGB Retrieval Model

Many models have been suggested for AGB retrieval from P-band backscatter and a power law has been shown to be a good first-order model. A power law is physically motivated as being representative of the backscatter from a vegetation layer of random scatterers, under the assumption of no attenuation or ground effects [25]. However, ground effects tend to give rise to significant variations in backscatter at P-band motivating modifications such as using γ^0 values, incorporating multiple polarizations, or ground slope-dependent terms [11]–[13].

In [21], it was found that a power law in the form of (1) performed well in retrieving AGB B from both L-band SAR (γ^0) and volumetric TomoSAR intensity (I_{vol}). The best performing L-band polarization components PQ were HV for SAR data and HH for TomoSAR data, although in the latter case all channels had similar performance

$$\hat{B} = \exp\left(a_0 + a_1\left[\gamma^0_{\text{PQ}}\right]_{dB}\right) + \epsilon$$
$$\hat{B} = \exp\left(b_0 + b_1\left[I_{\text{vol,PQ}}\right]_{dB}\right) + \epsilon. \quad (1)$$

Model parameters are obtained by nonlinear least-squares fitting (1) to training data from each data set. Formulating and training the model in this way ensures that the AGB estimates are bounded by the range of reference AGB for the backscatter intensity values within the range found in the data. The model also tends toward the best *a priori* estimate (i.e., average reference AGB) for noncorrelated observables. The model is linear in B which was found to minimize the resulting estimation error.

IV. Results

The strongest AGB dependence was found for the HV polarization in KR, which is consistent with previous findings at P-band. However, in RE the HH data performed slightly better than HV as can be seen by comparing the results in Table III. VV showed no useful correlation with AGB in either campaign.

A. Overview of Backscatter Variations in KR

Two regions of interest were selected to show the different spatial variations seen in the radar data and highlight the relative impact of vertical tomographic resolution, ground slope, and forest AGB on SAR and TomoSAR HV polarized backscatter intensity.

The first region, seen in Fig. 5, contains stand 2228 which is located in the middle of the swath resulting in similar vertical resolution and incidence angles for the two opposing flight headings. Backscatter intensities are mostly constant within the stand which is expected as the AGB map and DTM shows that this is an area of homogeneous forest in flat terrain on a slope perpendicular to the radar line of sight. A clearing just north of stand 2228 is clearly marked by low AGB values and correspondingly low backscatter.

TABLE III
Model Training Errors and Parameters for the RE HH and HV Polarized SAR and TomoSAR Training Data Sets

	Input	# of stands	RMSE [t/ha]	Bias [t/ha]	R^2	a_0	a_1
HH	γ^0	50	29.2 (24%)	-0.6	0.64	5.26	0.14
	I_{tot}	50	29.8 (25%)	-0.7	0.62	5.25	0.13
	I_{vol}	50	36.2 (30%)	-0.5	0.44	5.84	0.10
HV	γ^0	50	31.8 (26%)	-0.7	0.57	7.96	0.27
	I_{tot}	50	35.8 (30%)	-0.7	0.45	7.77	0.24
	I_{vol}	50	40.7 (34%)	-0.5	0.29	6.70	0.10

The difference between the data from the two opposing headings are highlighted in the third row of Fig. 5 which shows the ratio of NE to SW γ^0, I_{ground} and I_{vol}. An increase in NE backscatter and decrease in SW backscatter is found in two areas running along the longer stand edges more or less parallel to the flight tracks. There are no related forest features in the AGB map but these variations correspond to areas with sloping ground in the DTM. The best correlation is found with the ground slope in the line of sight, u_{LOS}, defined as the angle between the vertical unit vector and the surface normal projected onto a plane perpendicular to the flight track. Positive slope (toward the radar) results in increased backscatter and negative slope (away from radar) decreases backscatter. TomoSAR I_{ground} and SAR γ^0 are most heavily affected while the impact is smaller for I_{vol}.

The second region, shown in Fig. 6, is an area in the southeast corner of the swath with high incidence angles/low vertical resolution from the NE direction and correspondingly low incidence angles/high vertical resolution for the SW direction. This region contains stands 3245 and 32 398 which have high and low AGB averages of 167.1 and 27.5 t/ha, respectively. The large incidence angles in the NE data set produce a strong response for areas with positive u_{LOS} and AGB variations within the forested area are not well represented in NE backscatter data. Even though ground signal suppression for I_{vol} is limited by the poor vertical resolution the impact of ground slope is still decreased when compared with I_{ground} and γ^0.

With lower incidence angles and mainly negative slopes the SW looking data is less affected by topography and backscatter variations are more representative of AGB, especially for the lower AGB forest in stand 32 398. The improved tomographic resolution results in a larger difference between I_{vol} and I_{ground} than for the NE looking data. Comparing the two headings in row three of Fig. 6 shows that NE backscatter values are generally higher, with the difference being larger for TomoSAR I_{ground} and I_{vol}. There is a strong dependence on u_{LOS} for I_{ground} while I_{vol} has more of a constant offset.

A direct evaluation of the AGB dependence of the radar backscatter is found in Fig. 7, which plots average SAR

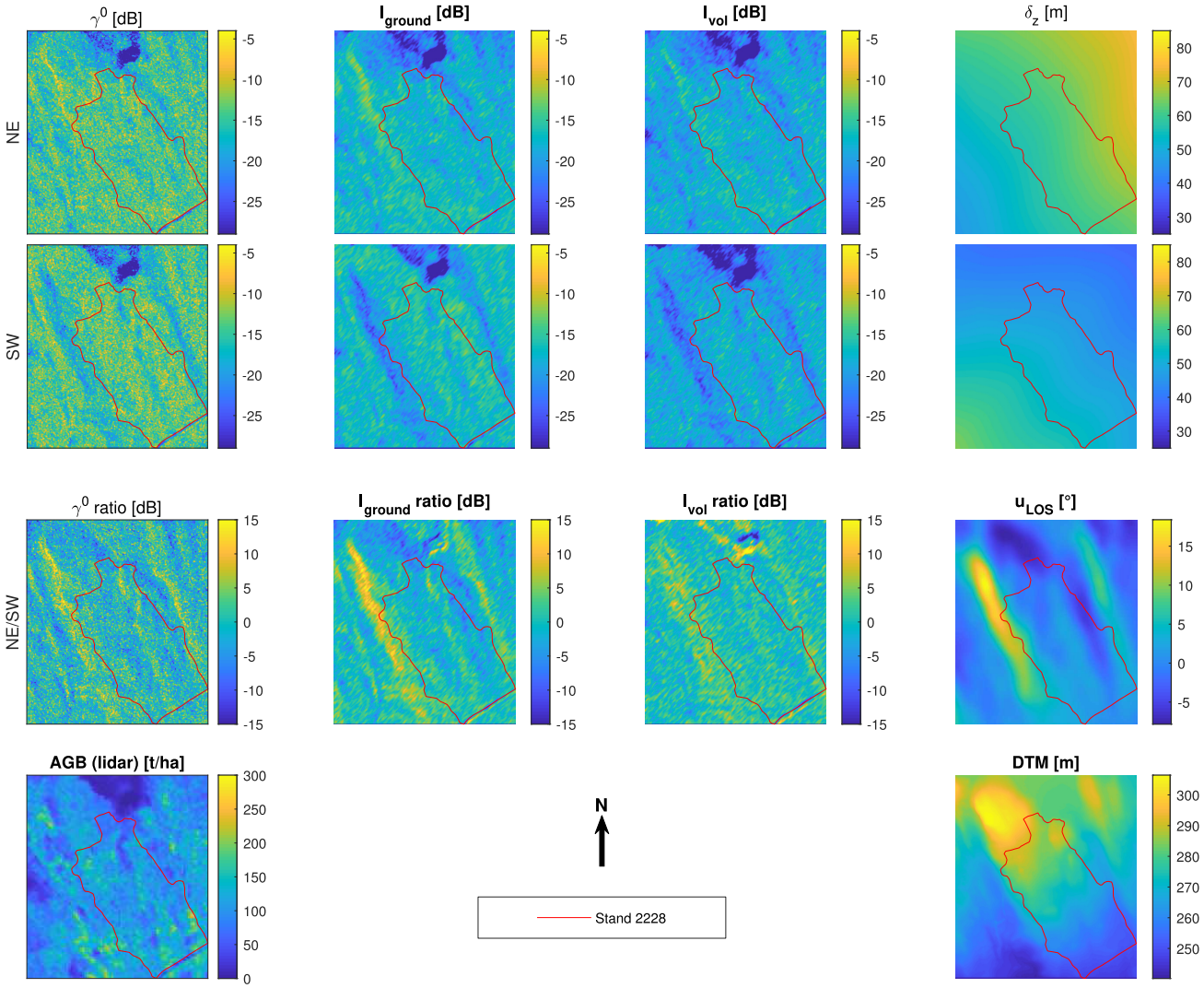

Fig. 5. Detailed data for the area around stand 2228. First three columns: HV polarized SAR intensity, TomoSAR ground, and TomoSAR volume intensity data for (Top) NE and (Second) SW look directions with the respective ratios in the third row. Fourth column: vertical tomographic resolution δ_z for the two directions and the ground slope in line of sight u_{LOS} (positive for NE). Last row: (Left) Lidar AGB and (Right) DTM. Imaged area is 912 m × 806 m.

and TomoSAR backscatter values for the circular plots and forest stands in KR. HV polarized SAR γ^0, shown in the first column, has a similar variation with AGB as the total tomographic backscatter I_{tot} shown in the second column. The third and fourth columns show the backscatter split into ground and volumetric components, respectively, using a $z = 10$ m threshold. I_{vol} has the largest dynamic range and is less affected by factors other than AGB compared to the other TomoSAR observables, with I_{ground} exhibiting the opposite behavior with more widely distributed intensity values. NE looking data show a stronger AGB dependence compared to SW looking data, especially for high AGB values.

B. Impact of Vertical Resolution in KR

The vertical tomographic resolution δ_z varies with range for all the data sets, especially in KR where it goes from typical forest height (20 m) to more than five times larger at far range. The impact of this variation is seen in Fig. 8 which shows the parameters and errors obtained when fitting (1) to SAR γ^0 and TomoSAR I_{vol}, plotted as a function of the vertical resolution δ_z. The 517 circular plots were grouped into five bins based on vertical resolution with 103–104 plots per bin.

Fitted parameters are similar at low values of δ_z with the difference and resulting error increasing with increasing δ_z for both SAR and TomoSAR data. I_{vol} consistently gives smaller errors when compared to γ^0, converging with the SAR performance with decreasing vertical resolution. The divergence of the fitted model parameters and increasing error for values of δ_z higher than 50–60 m motivated a restriction to some minimum resolution. Restricting the incidence angle to the 25°–35° range to match the planned BIOMASS acquisition geometry gives a worst-case resolution of 38 m and will thus also ensure that the tomographic resolution is good enough for meaningful TomoSAR performance with these observables.

C. AGB Retrieval in KR

Fitting (1) to the 138 (NE) and 94 (SW) circular plots in the near range quarter of each scene (incidence angle of 25°–35°)

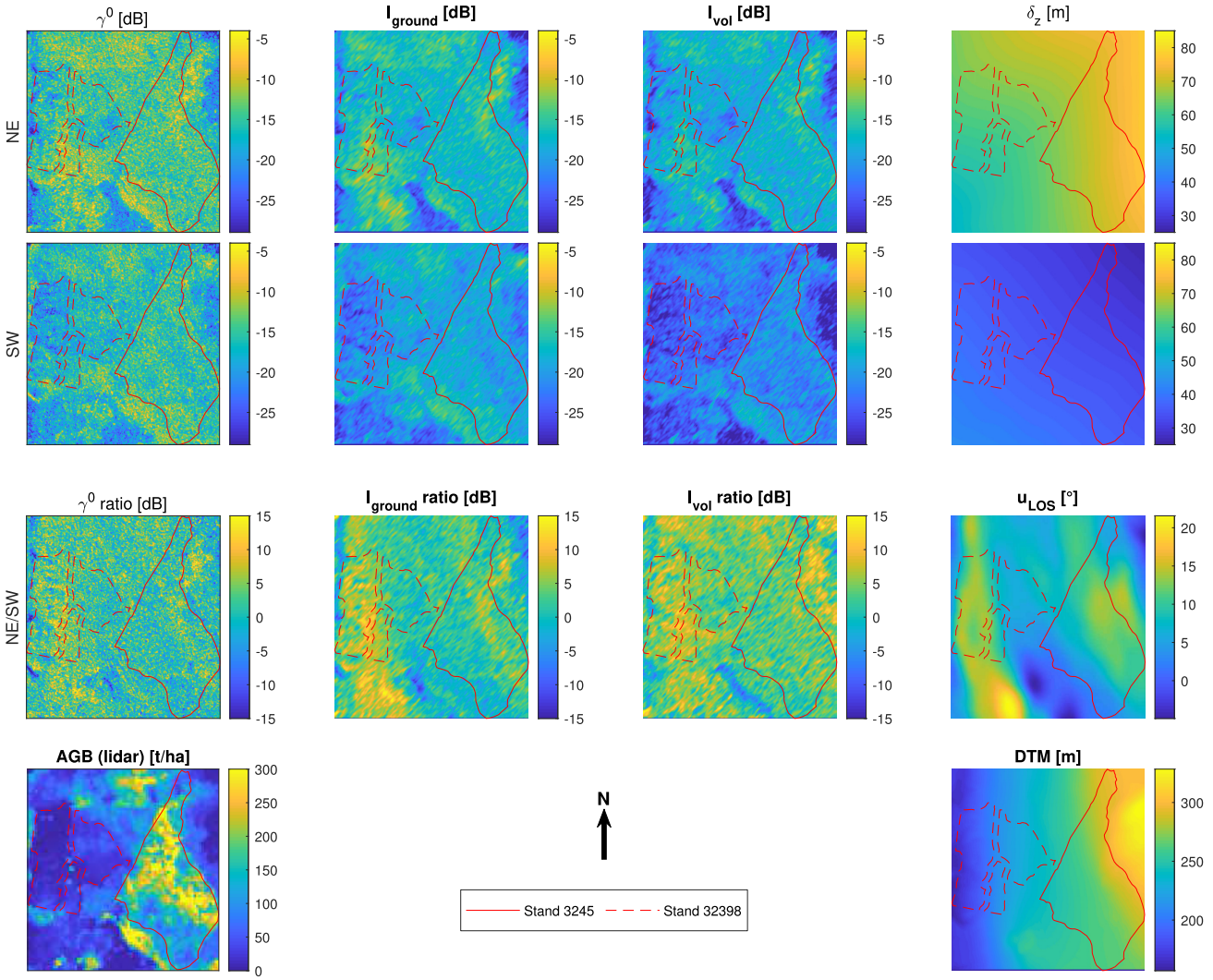

Fig. 6. Detailed data for stands 3245 and 32 398. First three columns: HV polarized SAR intensity, TomoSAR ground and TomoSAR volume intensity data for (Top) NE and (second) SW look directions with the respective ratios in the third row. Fourth column: vertical tomographic resolution δ_z for the two directions and the ground slope in line of sight u_{LOS} (positive for NE). Last row: (Left) Lidar AGB and (Right) DTM. Imaged area is 761 m $\times$ 727 m.

results in the AGB retrievals shown in Figs. 9, 10, and 11, with all fitted parameters and average errors displayed in Table IV. The results in Fig. 10 use the full airborne resolution SAR and TomoSAR data, showing that TomoSAR I_{tot} gives similar, if slightly larger, residuals as γ^0 while TomoSAR I_{vol} shows an significant improvement. The NE data set consistently result in better training residuals and retrievals, however the number of forest stands in each region is 10 (NE) and 3 (SW) making statistically significant validation difficult for the SW data set.

Using 6-MHz bandwidth and restricting the incidence angle to 25°–35° gives a data set representative of BIOMASS except for the airborne geometry (see Section III-A) and results in the retrievals shown in Fig. 11. The performance is close to that using airborne data reflecting that the vertical resolution of the airborne data is limited by the geometry while showing that the size of the circular plots is large enough to produce good averages despite the reduced horizontal resolution.

Table IV contains an overview of error statistics and parameters when fitting the AGB retrieval model to the SAR and TomoSAR observables for the training data sets in KR.

A detailed view of the model training errors is obtained by sorting the circular plots by AGB into bins of 50 t/ha, lower bound inclusive, with the fourth bin containing all plots with AGB $\geq$ 150 t/ha. This results in a distribution of [53, 42, 31, 12] circular plots for the NE data and [30, 39, 17, 8] circular plots for the SW data. AGB retrieval model training residual bias, standard deviation, and root mean squared error (RMSE) are plotted against bin average AGB in Fig. 9. SAR γ^0 and TomoSAR I_{tot} show no significant differences while I_{vol} has a consistently lower bias and RMSE, especially for the lowest and highest AGB values. The improvement is more pronounced for the NE looking data set.

D. AGB Dependence and Retrieval in RE

Fig. 12 shows the HH polarized backscatter dependence on AGB for the RE data set. The resolution in RE is 55 m or better for the whole swath which made it unnecessary to limit the incidence angle range, especially considering the limited extent of the stand reference data. TomoSAR backscatter has

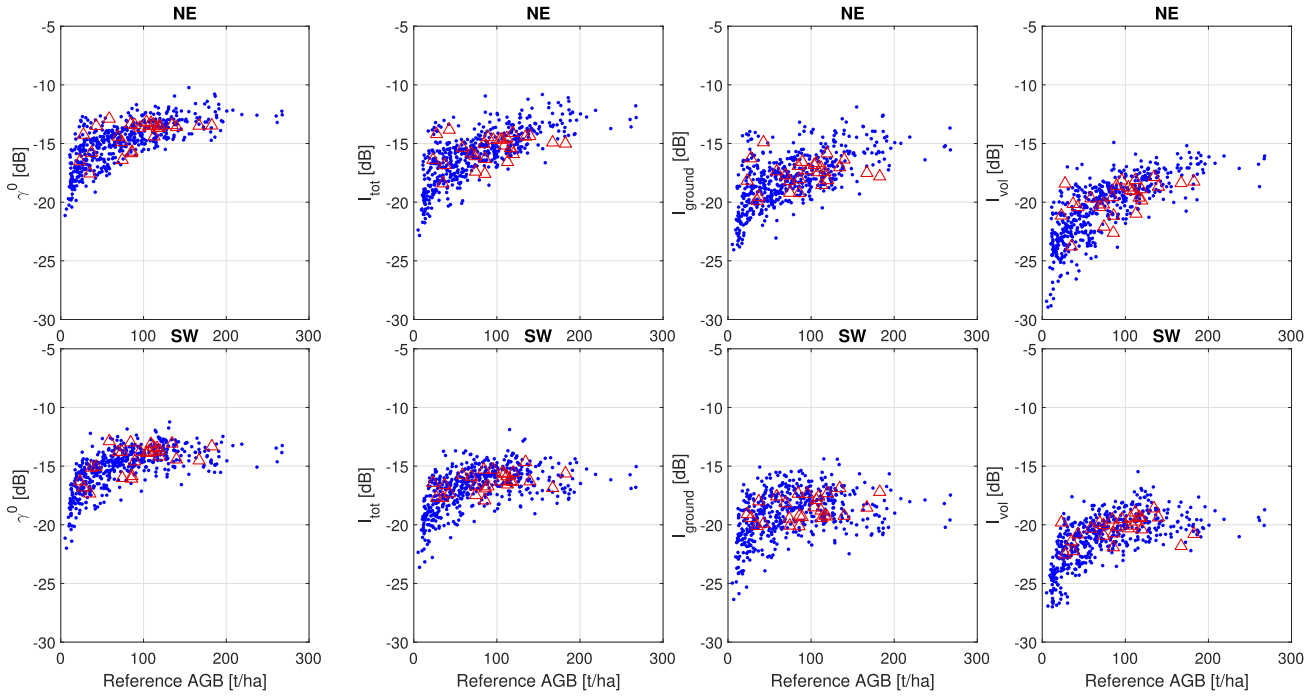

Fig. 7. SAR and TomoSAR HV polarized backscatter intensity as function of AGB for (Top) north-east looking and (Bottom) south-west looking directions. (Left to right) SAR γ^0, total tomographic intensity, ground intensity ($z = -10$ m to $z = 10$ m) and volumetric intensity ($z = 10$ m to $z = 30$ m). Points and triangles correspond to plots and stands shown in Fig. 3.

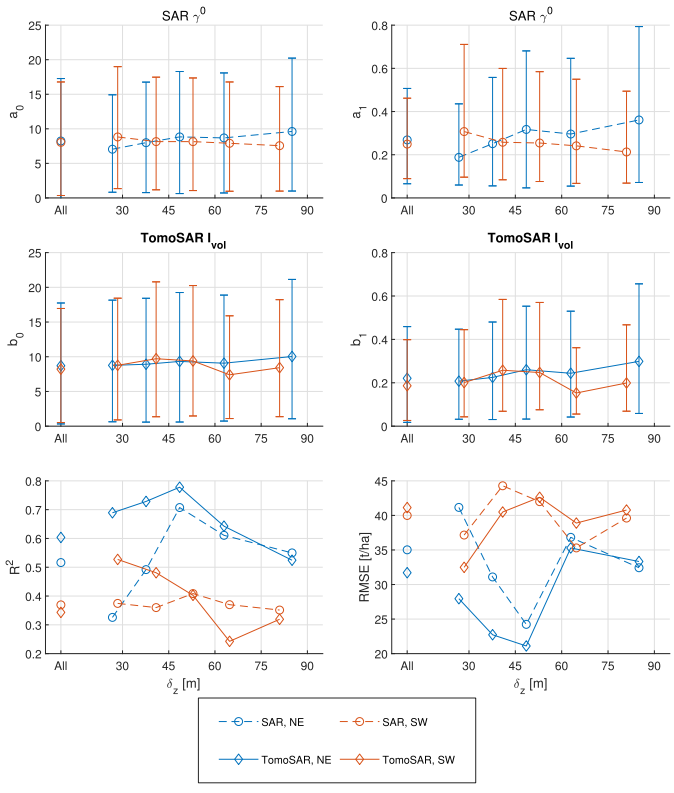

Fig. 8. AGB retrieval model parameters and errors when fitting the training data split into 5 δ_z bins (103–104 plots per bin).

a similar dynamic range and dispersion compared to SAR γ^0. I_{tot} and I_{ground} backscatter values are almost identical with I_{vol} having a lower intensity and slightly larger dispersion.

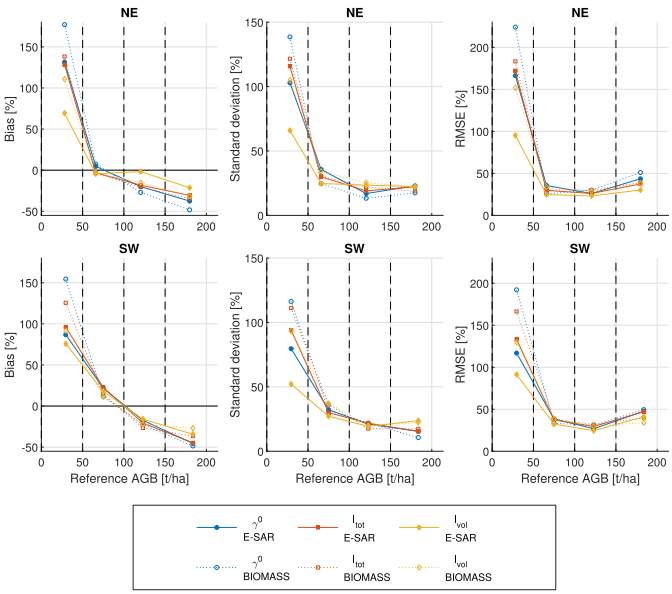

Fig. 9. AGB dependent variation in the relative bias, standard deviation and RMSE for the model training residuals shown in Figs. 10 and 11. The circular plots were grouped into four bins based on AGB (<50, 50-100, 100-150, ≥150 t/ha) and retrieval error statistics, normalized by reference AGB, were computed for each of the SAR and TomoSAR observables.

Using data from 50 of the forest stands to fit (1) and using the ten square plots for validation results in the AGB retrievals displayed in Table III for HH and HV polarization with HH retrieval results seen in Fig. 13.

V. Discussion

The relatively flat terrain in RE demonstrates the case when the backscattered power is not strongly modulated by

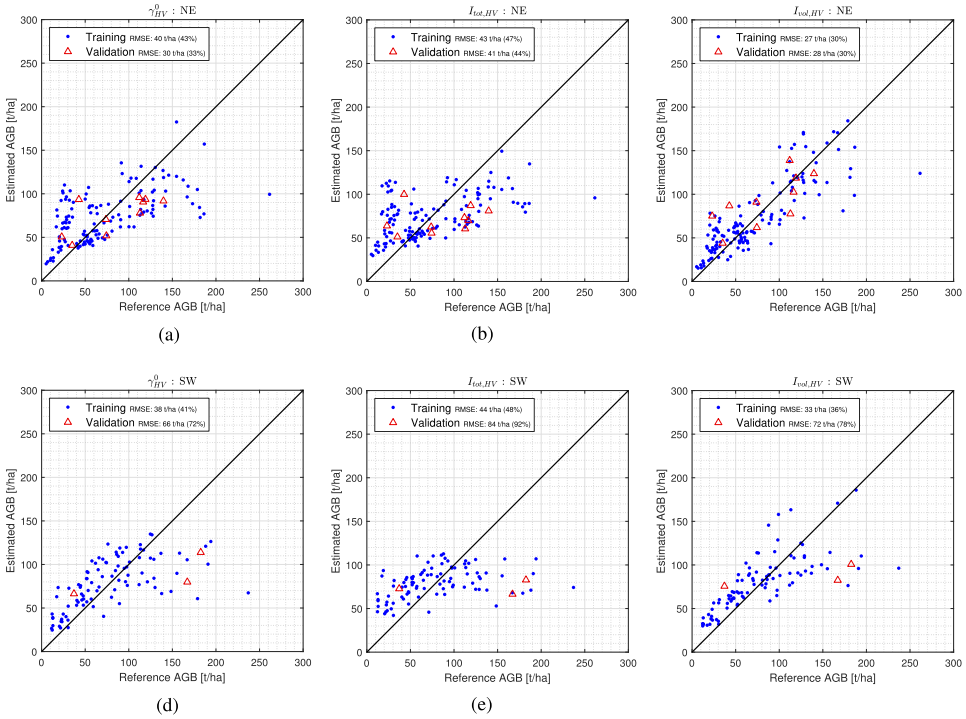

Fig. 10. SAR γ^0 and TomoSAR I_{tot} and I_{vol} training and validation AGB retrievals for airborne HV polarized data when incidence angles are 25°–35°. Points and triangles correspond to plots and stands shown in Fig. 3. (a) AGB retrieval using NE SAR γ^0. (b) AGB retrieval using NE TomoSAR I_{tot}. (c) AGB retrieval using NE TomoSAR I_{vol}. (d) AGB retrieval using SW SAR γ^0. (e) AGB retrieval using SW TomoSAR I_{tot}. (f) AGB retrieval using SW TomoSAR I_{vol}.

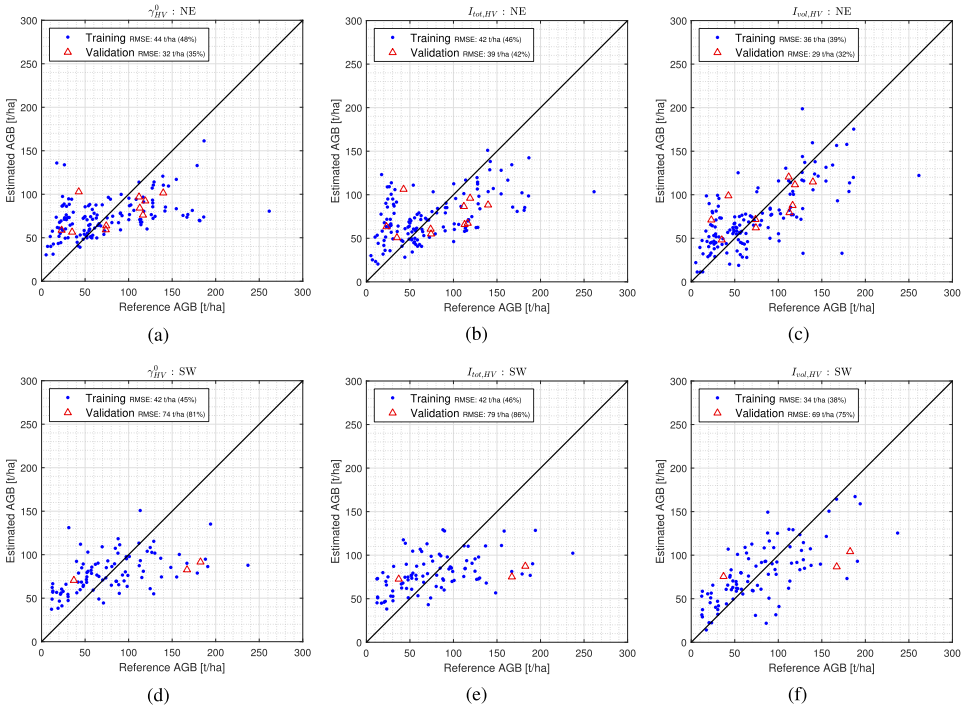

Fig. 11. SAR γ^0 and TomoSAR I_{tot} and I_{vol} training and validation AGB retrievals for simulated BIOMASS HV polarized data. Points and triangles correspond to plots and stands shown in Fig. 3. (a) AGB retrieval using NE SAR γ^0. (b) AGB retrieval using NE TomoSAR I_{tot}. (c) AGB retrieval using NE TomoSAR I_{vol}. (d) AGB retrieval using SW SAR γ^0. (e) AGB retrieval using NE TomoSAR I_{tot}. (f) AGB retrieval using SW TomoSAR I_{vol}.

sloping ground. There is little difference in the distribution of volume and ground intensity and removing the strong ground level contribution increases noise and has a net negative effect on performance.

There is a marked difference between the two opposing imaging directions in KR, with the NE data set producing the best retrievals for both SAR and TomoSAR data. The only difference in image acquisition geometries is the

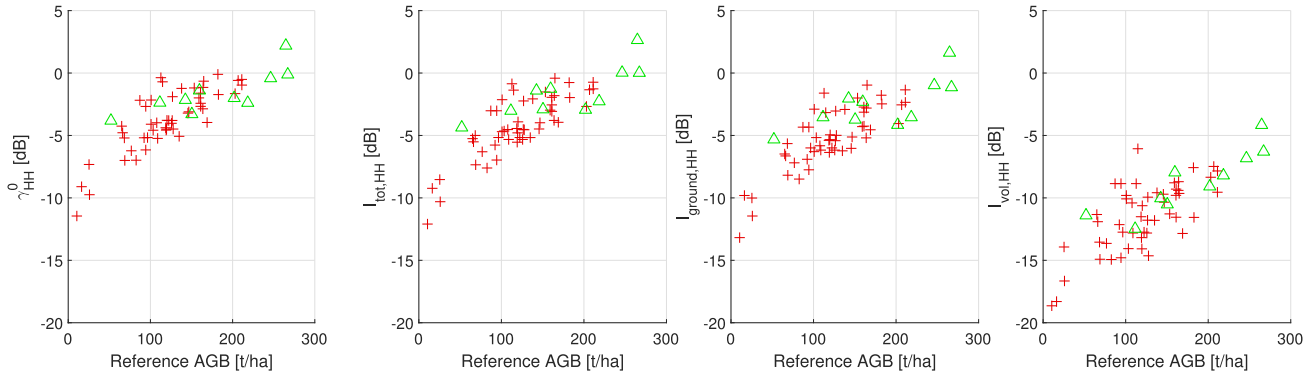

Fig. 12. SAR and tomographic HH polarized backscatter intensity as function of biomass in RE. (Left to right) SAR γ^0, total tomographic intensity, ground intensity ($z = -10$ m to $z = 10$ m) and volumetric intensity ($z = 10$ m to $z = 30$ m). Forest stands are marked in red while the square plots are marked in green.

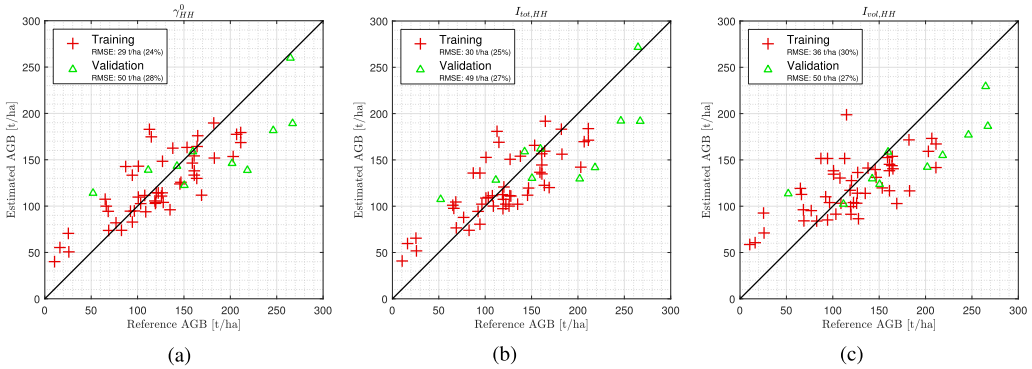

Fig. 13. AGB model training residuals obtained for the stands in RE. Forest stands are marked in red while the square plots are marked in green. (a) AGB retrieval using SAR γ^0. (b) AGB retrieval using TomoSAR I_{tot}. (c) AGB retrieval using TomoSAR I_{vol}.

opposing headings suggesting that these deviations are caused by systematic variations in the scene. This is highlighted by the RMSE values seen in Fig. 8 (bottom right) where the largest difference between NE and SW is found in the middle bin, which corresponds to the mostly overlapping region in the center of the swath and close to identical illumination angles from the two headings.

Comparing the model parameters obtained for SAR γ^0 in Fig. 8 (top row) for the two headings they appear to show a mirrored dependence on vertical tomographic resolution δ_z. Attainable tomographic resolution is irrelevant for single SAR images but is in this case a close proxy for incidence angle and ground range. A lack of direct correlation with δ_z therefore indicates that the corrections for incidence angle used in computing γ^0 are sufficient. As the axis of increasing δ_z represents opposing directions in the scene for the two headings it is clear both data sets result in similar fits with model parameters a_0 and a_1 increasing slightly from the NE flight line toward the SW flight line (i.e., toward the north-east edge of the swath). This would indicate a gradient in some relevant property of the imaged scene, such as the AGB distribution or topography.

Using the γ^0 normalization for SAR intensity data will also introduce a first-order compensation for the effect of ground slope. Models including a ground slope-dependent term in combination with more polarimetric data are able to improve results further [12] but the complex interactions between the forest and the ground generally leads to rapidly diminishing returns when including more model parameters. Adequate ground slope angle information also requires high-resolution DTM data [14] which can represent a serous operational challenge.

Fitting I_{vol} results in more consistent parameters, as long as the vertical resolution is sufficient, as seen in the second row of Fig. 8. This is indicative of the improved retrievals seen with TomoSAR data and further suggest that the across track variations in fitted SAR model parameters are related to ground level backscatter. Neither AGB nor ground slope u_{LOS} values of the plots show any significant correlation with across track position in the imaged area and cannot directly explain these differences.

However, there is a significant directional bias of 1.6° in u_{LOS} plot values which could be a contributing factor to the RMSE differences. Fig. 14 shows the ground slope for the subsets of 138 (NE) and 94 (SW) circular plots which averages to 1.1° and 2.4°, respectively, both toward the NE flight line. For the NE plots, there is also a positive correlation between AGB and u_{LOS} which would reinforce any adverse effects on AGB retrieval errors.

An important factor of the improvement seen with I_{vol} is reduced bias. While the AGB models minimizes total bias for all observables Fig. 9 shows that I_{vol} has smaller relative

TABLE IV
MODEL TRAINING ERRORS AND PARAMETERS FOR THE DIFFERENT SAR AND TOMOSAR KR HV TRAINING DATA SETS

	Input		# of plots	# of stands	RMSE [t/ha]	Bias [t/ha]	R^2	a_0	a_1
γ^0	All data	(NE)	517	27	35.0 (38%)	-0.6	0.52	8.24	0.27
		(SW)	517	27	40.0 (44%)	-0.8	0.37	8.04	0.25
	$25° \leq \theta_i \leq 35°$	(NE)	138	10	39.5 (43%)	-0.4	0.37	7.30	0.20
		(SW)	94	3	37.6 (41%)	-0.4	0.39	8.68	0.30
	BIOMASS	(NE)	138	10	44.3 (48%)	-0.4	0.21	6.05	0.12
		(SW)	94	3	41.6 (45%)	-0.5	0.25	6.30	0.14
I_{tot}	All data	(NE)	517	27	40.6 (44%)	-0.7	0.35	6.66	0.16
		(SW)	517	27	48.0 (52%)	-0.2	0.10	5.93	0.10
	$25° \leq \theta_i \leq 35°$	(NE)	138	10	42.9 (47%)	-0.3	0.26	6.15	0.13
		(SW)	94	3	44.0 (48%)	-0.2	0.17	6.68	0.16
	BIOMASS	(NE)	138	10	42.0 (46%)	-0.1	0.29	6.82	0.15
		(SW)	94	3	42.3 (46%)	-0.3	0.23	7.12	0.17
I_{vol}	All data	(NE)	517	27	31.7 (35%)	-0.3	0.60	8.71	0.22
		(SW)	517	27	41.1 (45%)	-0.8	0.34	8.22	0.19
	$25° \leq \theta_i \leq 35°$	(NE)	138	10	27.4 (30%)	-0.7	0.70	8.62	0.20
		(SW)	94	3	32.9 (36%)	-1.1	0.54	8.66	0.19
	BIOMASS	(NE)	138	10	35.6 (39%)	0.3	0.49	8.10	0.17
		(SW)	94	3	34.5 (38%)	0.4	0.49	9.34	0.22

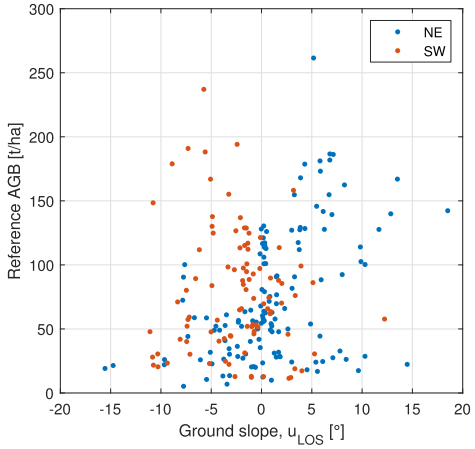

Fig. 14. AGB as a function of plot average ground slope in the line of sight, u_{LOS}, for the subsets of plots used for AGB model training in KR.

bias over the whole AGB range with the NE data set having negligible bias for the center of the AGB distribution. The largest relative differences between the observables are seen for small AGB values which represent a small fraction of total AGB in KR but are important for determining the sensitivity of the AGB retrieval.

Simulated BIOMASS I_{vol}, while an clear improvement over BIOMASS γ^0, result in errors close to that of E-SAR γ^0 rather than E-SAR I_{vol}. As the vertical tomographic resolution is similar in this case due to the geometry this should be directly related to the reduction in horizontal resolution. This suggest that while inhomogeneities in the vegetation layer can be resolved in the high-resolution E-SAR data these variations do not contribute linearly toward AGB retrieval from P-band TomoSAR when the resolution is lowered. Further work is needed to determine the relative importance of vertical and horizontal resolution for tomographic data and to investigate whether improvements can be made through changes to the tomographic processing or AGB retrieval models.

VI. CONCLUSION

While tomographic processing of P-band SAR data has shown promise with regard to AGB retrieval in tropical forest the case for boreal forest is challenging. The limited vertical extent of the forest, generally less than the bandwidth limited resolution that will be available for BIOMASS, limits the possibility to resolve the vertical forest structure. At the same time, the ground level reflection is relatively strong as well as highly sensitive to ground slope which conspire to mask the AGB signal in the measurements.

Using tomographic processing to suppress the HV ground signal is effective for KR with its varying topography as long as the resolution is no worse than about twice the forest height. TomoSAR data representative of BIOMASS result in errors on par with high resolution airborne E-SAR data while the corresponding airborne TomoSAR data suggest that further improvements might be possible, especially regarding a reduction of AGB retrieval bias over the whole AGB range.

In areas of flat terrain, such as the forest imaged in RE, the AGB retrievals based on P-band SAR data perform better and the suppression of the ground signal at HH or HV introduces more variability with little benefit. Future studies might focus on finding parameters related to vertical forest structure while minimizing requirements on vertical resolution to be relevant for future acquisitions.

REFERENCES

[1] Food and Agriculture Organization of the United Nations (FAO), Rome, Italy. (2016). *The Global Forest Resources Assessment 2015*. [Online]. Available: http://www.fao.org/3/a-i4793e.pdf

[2] Y. Su *et al.*, "Spatial distribution of forest aboveground biomass in China: Estimation through combination of spaceborne lidar, optical imagery, and forest inventory data," *Remote Sens. Environ.*, vol. 173, pp. 187–199, Feb. 2016, doi: 10.1016/j.rse.2015.12.002.

[3] M. C. Dobson, F. T. Ulaby, T. LeToan, A. Beaudoin, E. S. Kasischke, and N. Christensen, "Dependence of radar backscatter on coniferous forest biomass," *IEEE Trans. Geosci. Remote Sens.*, vol. 30, no. 2, pp. 412–415, Mar. 1992. [Online]. Available: http://ieeexplore.ieee.org/document/134090/

[4] T. Le Toan, A. Beaudoin, J. Riom, and D. Guyon, "Relating forest biomass to SAR data," *IEEE Trans. Geosci. Remote Sens.*, vol. 30, no. 2, pp. 403–411, Mar. 1992. [Online]. Available: http://ieeexplore.ieee.org/document/134089/

[5] A. Reigber and A. Moreira, "First demonstration of airborne SAR tomography using multibaseline L-band data," *IEEE Trans. Geosci. Remote Sens.*, vol. 38, no. 5, pp. 2142–2152, Sep. 2000. [Online]. Available: http://ieeexplore.ieee.org/document/868873/

[6] O. Frey and E. Meier, "Analyzing tomographic SAR data of a forest with respect to frequency, polarization, and focusing technique," *IEEE Trans. Geosci. Remote Sens.*, vol. 49, no. 10, pp. 3648–3659, Oct. 2011. [Online]. Available: http://ieeexplore.ieee.org/document/5751670/

[7] M. Neumann, S. S. Saatchi, L. M. H. Ulander, and J. E. S. Fransson, "Assessing performance of L- and P-band polarimetric interferometric SAR data in estimating boreal forest above-ground biomass," *IEEE Trans. Geosci. Remote Sens.*, vol. 50, no. 3, pp. 714–726, Mar. 2012. [Online]. Available: http://ieeexplore.ieee.org/lpdocs/epic03/wrapper.htm?arnumber=6129499

[8] M. M. d'Alessandro, S. Tebaldini, and F. Rocca, "Phenomenology of ground scattering in a tropical forest through polarimetric synthetic aperture radar tomography," *IEEE Trans. Geosci. Remote Sens.*, vol. 51, no. 8, pp. 4430–4437, Aug. 2013. [Online]. Available: http://ieeexplore.ieee.org/lpdocs/epic03/wrapper.htm?arnumber=6484135

[9] O. Ponce, P. Prats-Iraola, R. Scheiber, A. Reigber, and A. Moreira, "First airborne demonstration of holographic SAR tomography with fully polarimetric multicircular acquisitions at L-band," *IEEE Trans. Geosci. Remote Sens.*, vol. 54, no. 10, pp. 6170–6196, Oct. 2016. [Online]. Available: http://ieeexplore.ieee.org/document/7517224/

[10] ESA, "Report for mission selection: Biomass," Eur. Space Agency, Noordwijk, The Netherlands, Tech. Rep. ESA SP-1324/1 (3 volume series), 2012. [Online]. Available: https://esamultimedia.esa.int/docs/EarthObservation/SP1324-1_BIOMASSr.pdf

[11] G. Sandberg, L. M. H. Ulander, J. E. S. Fransson, J. Holmgren, and T. Le Toan, "L- and P-band backscatter intensity for biomass retrieval in hemiboreal forest," *Remote Sens. Environ.*, vol. 115, no. 11, pp. 2874–2886, Nov. 2011, doi: 10.1016/j.rse.2010.03.018.

[12] M. J. Soja, G. Sandberg, and L. M. H. Ulander, "Regression-based retrieval of boreal forest biomass in sloping terrain using P-band SAR backscatter intensity data," *IEEE Trans. Geosci. Remote Sens.*, vol. 51, no. 5, pp. 2646–2665, May 2013.

[13] M. Schlund, K. Scipal, and S. Quegan, "Assessment of a power law relationship between P-band SAR backscatter and aboveground biomass and its implications for BIOMASS mission performance," *IEEE J. Sel. Topics Appl. Earth Observ. Remote Sens.*, vol. 11, no. 10, pp. 3538–3547, Oct. 2018. [Online]. Available: https://ieeexplore.ieee.org/document/8462721/

[14] B. Hallberg, G. Smith-Jonforsen, L. M. H. Ulander, and G. Sandberg, "A physical-optics model for double-bounce scattering from tree stems standing on an undulating ground surface," *IEEE Trans. Geosci. Remote Sens.*, vol. 46, no. 9, pp. 2607–2621, Sep. 2008.

[15] M. J. Soja, G. Sandberg, and L. M. H. Ulander, "Topographic correction for biomass retrieval from P-band SAR data in boreal forests," in *Proc. IEEE Int. Geosci. Remote Sens. Symp.*, Jul. 2010, pp. 4776–4779.

[16] D. Ho Tong Minh, T. L. Toan, F. Rocca, S. Tebaldini, M. M. d'Alessandro, and L. Villard, "Relating P-band synthetic aperture radar tomography to tropical forest biomass," *IEEE Trans. Geosci. Remote Sens.*, vol. 52, no. 2, pp. 967–979, Feb. 2014. [Online]. Available: http://ieeexplore.ieee.org/lpdocs/epic03/wrapper.htm?arnumber=6488809

[17] D. Ho Tong Minh, S. Tebaldini, F. Rocca, T. Le Toan, L. Villard, and P. C. Dubois-Fernandez, "Capabilities of BIOMASS tomography for investigating tropical forests," *IEEE Trans. Geosci. Remote Sens.*, vol. 53, no. 2, pp. 965–975, Feb. 2015. [Online]. Available: http://ieeexplore.ieee.org/document/6849523/

[18] I. Hajnsek *et al.*, "BioSAR 2007. Technical assistance for the development of airborne SAR and geophysical measurements during the BioSAR 2007 experiment: Final report without synthesis," Eur. Space Agency, Paris, France, Tech. Rep., 2008.

[19] I. Hajnsek *et al.* (2009). *BIOSAR 2008: Final Report*. [Online]. Available: https://earth.esa.int/c/document_library/get_file?folderId=21020&name=DLFE-903.pdf

[20] M. J. Soja, H. J. Persson, and L. M. H. Ulander, "Estimation of forest biomass from two-level model inversion of single-pass InSAR data," *IEEE Trans. Geosci. Remote Sens.*, vol. 53, no. 9, pp. 5083–5099, Sep. 2015. [Online]. Available: http://ieeexplore.ieee.org/document/7094294/

[21] E. Blomberg, L. Ferro-Famil, M. J. Soja, L. M. H. Ulander, and S. Tebaldini, "Forest biomass retrieval from L-band SAR using tomographic ground backscatter removal," *IEEE Geosci. Remote Sens. Lett.*, vol. 15, no. 7, pp. 1030–1034, Jul. 2018. [Online]. Available: https://ieeexplore.ieee.org/document/8336957/

[22] S. Tebaldini, F. Rocca, M. Mariotti d'Alessandro, and L. Ferro-Famil, "Phase calibration of airborne tomographic SAR data via phase center double localization," *IEEE Trans. Geosci. Remote Sens.*, vol. 54, no. 3, pp. 1775–1792, Mar. 2016. [Online]. Available: http://ieeexplore.ieee.org/document/7308057/

[23] L. M. H. Ulander, "Radiometric slope correction of synthetic-aperture radar images," *IEEE Trans. Geosci. Remote Sens.*, vol. 34, no. 5, pp. 1115–1122, Sep. 1996.

[24] R. K. Raney, T. Freeman, R. W. Hawkins, and R. Bamler, "A plea for radar brightness," in *Proc. IGARSS-IEEE Int. Geosci. Remote Sens. Symp.*, Aug. 1994, pp. 1090–1092.

[25] M.-L. Truong-Loi, S. Saatchi, and S. Jaruwatanadilok, "Soil moisture estimation under tropical forests using UHF radar polarimetry," *IEEE Trans. Geosci. Remote Sens.*, vol. 53, no. 4, pp. 1718–1727, Apr. 2015. [Online]. Available: http://ieeexplore.ieee.org/document/6882797/